IR-SPECTROSCOPY, THERMOPHYSICAL AND MECHANICAL PROPERTIES OF GLASSES IN THE SYSTEM $Na_2O/BaO/TiO_2/B_2O_3/SiO_2/Al_2O_3$

Ruzha Harizanova[1], Valentin Gaydarov[2], Ivailo Gugov[1], Galina Zamfirova[2], Irena Mihailova[1], Martin Pernikov[1], Christian Rüssel[3]

[1]*University of Chemical Technology and Metallurgy*
8 Kliment Ohridski blvd., 1756 Sofia, Bulgaria
[2]*"Todor Kableshkov" University of Transport*
158 Geo Milev str., 1574 Sofia, Bulgaria
[3]*Otto Schott Institute of Materials Research*
Jena University, Fraunhoferstr. 6,07743 Jena, Germany
E-mail: rharizanova@uctm.edu

Received 22 December 2022
Accepted 10 January 2023

ABSTRACT

Glasses with the compositions (23.1-x)Na_2O/23.1BaO/23TiO_2/9.8B_2O_3/21SiO_2/xAl_2O_3 x = 3, 7, 11 and 15 mol% were melted using a traditional melt-quenching technique. The thermophysical properties of the obtained glasses, i.e., glass transition temperature, T_g, and crystallization peak maximum temperature, T_c, were determined by differential scanning calorimetry and showed that the increasing alumina concentration leads to an increase of both the T_g and T_c values, while the difference T_g-T_c, used as a glass stability criterium, changes in the opposite manner, being highest for the glass with 3 mol % Al_2O_3 and smallest for the composition with 15 mol % Al_2O_3. The structure of the prepared series of glasses was studied by infrared spectroscopy and showed that the main structural units present are isolated and interconnected SiO_4 tetrahedra. Both BO_4 and BO_3 structural units, which number initially increases with the increasing alumina concentration and then starts to decrease, are also present. The conducted depth-sensing indentation on the obtained glasses allowed to determine mechanical properties such as universal (HMV) and indentation (Hit) hardness, elastic modulus and elastic part of indentation work. The change of the Na_2O/Al_2O_3 ratio resulted in increasing HMV and H_{it} up to 11 mol% Al_2O_3 and then a slight decrease of the respective parameters was observed.

Keywords: oxide glass, IR spectroscopy, DSC, glass transition temperature, micromechanical properties.

INTRODUCTION

The preparation of dielectric materials from oxide glasses via controlled crystallization has been reported for many years [1 - 4]. Here, the main approach is the choice of a well-studied parent glass to which the components from which the dielectric phase will crystallize are added. Frequently, also the effect of the latter components on the glass structure and the crystallization behavior was studied [1]. A versatile strategy for the crystallization of dielectric phases from oxide glasses is to choose a parent glass composition which tends to liquid/liquid phase separation. Here, the composition should be chosen in such a manner that one phase mainly consists of the constituting elements of the dielectric phase and in the second phase all other glass components are enriched [1 - 3]. One dielectric phase which was successfully precipitated from oxide glasses via controlled crystallization is barium titanate, $BaTiO_3$ [2 - 4]. In the past few decades, $BaTiO_3$ has frequently been studied and reported to be one of the best dielectric materials for energy storage. $BaTiO_3$ is used in various devices finding applications in electronics, sensor technology as well as in energy storage [4 - 9]. $BaTiO_3$ can be modified by doping with various other compounds, as for example with iron oxides. The as prepared materials received much attention due to their tunable dielectric and magnetic properties. They can find application in microelectronics for the elaboration of magnetic memories and switches [7, 8].

The possible applications of the barium titanate containing materials are determined by the respective phase in which $BaTiO_3$ occurs. There are four allotropic modifications of $BaTiO_3$ which in a different extent, exhibit useful properties such as piezoelectricity, pyroelectricity and ferroelectricity. Above the Curie temperature (120°C - 130°C), $BaTiO_3$ occurs in its cubic modification [2 - 6]. In this lattice, Ba^{2+} ions occupy the edges of the cubic cell, Ti^{4+} ions are centered in the cross-section of the space diagonals and O^{2-} are centered at the faces of the cube. Due to its cubic symmetry, $BaTiO_3$ is an isotropic dielectric phase and exhibits paraelectric properties. Below the Curie temperature, the $BaTiO_3$ structure transforms to a tetragonal one in which the Ba^{2+} and O^{2-} ions are located at the edges and the face centers, respectively, while the Ti^{4+} ions are no longer in the body center, but are shifted to the (001) - or $(00\bar{1})$ - plane. Hence, a dipolar moment parallel to the c-axis appears. This dipolar moment will lead to spontaneous polarization and thus, to ferroelectric and piezoelectric properties. Further decrease of temperature results in the transition from the tetragonal to an orthorhombic modification at approximately 0°C and from the orthorhombic into the rhombohedral phase at –90°C [4 - 6]. At temperatures higher than 1460°C a fifth allotropic modification of $BaTiO_3$ occurs - the hexagonal one [7], which can be stabilized even at room temperature by doping of the $BaTiO_3$ crystals with iron [7, 9]. The phase transition temperatures can widely be affected by substitution of Ba^{2+} with other divalent or even trivalent cations or of Ti^{4+} by tri-, tetra- or pentavalent cations. Furthermore, also the size and method of preparation of the $BaTiO_3$ crystals or their solid solutions might affect the phase formation [4 - 9]. The preparation method is usually an important factor which strongly influences the structure and the properties of materials. Traditionally, barium titanate is prepared via solid state syntheses at very high temperature [7, 8] or sol-gel methods [6] which often leads to inhomogeneities in the composition and the structure and to impurities due to unreacted precursors. Thus, alternative synthesis methods should be used in order to prepare materials with high purity, homogeneous particle distribution in the material volume and with a controllable degree of crystallinity. Such a method, combining these advantages, is the crystallization of barium titanate from oxide glasses [2 - 4, 9].

With respect to the potential practical application of oxide glasses and glass-ceramics in electronics and in sensor technology, the knowledge about their thermophysical and mechanical properties as well as dielectric properties is of great importance. This was already discussed in [10 - 13] for the cases of glasses and glass-crystalline or ceramic materials, containing $BaTiO_3$, barium titanate-based crystals or amorphous materials with high concentrations of BaO and TiO_2. For example, Vinothkumar et al. studied a Li^+ and Ba^{2+} ions doped B_2O_3 glass, in which the metal ions occupy positions leading to depolymerization of the glass network [14]. It is further concluded that structurally, the presence of alkali and alkali earth oxides in the composition of the respective glass will convert some of the BO_3 structural units into BO_4^- tetrahedra. This process will result in the linkage of metal ions in the glass structure. Increasing concentrations of BO_4^- units result in higher Young's moduli and higher density. Furthermore, it was reported in this work that 30 - 40 mol % alkali and other metal oxides lead to BO_4^- concentrations equal to those of BO_3. When, however, the concentration of the metal oxides exceeds 40 mol %, the number of BO_4^- units will decrease again which leads to the formation of non-bridging oxygens which also affects the mechanical properties of the glass.

The goal of the present work was to prepare a glass starting from a well-studied system, $Na_2O/B_2O_3/SiO_2/Al_2O_3$ to which large concentrations of BaO and TiO_2 are added. The reason is that from such compositions, the preparation of glass-ceramic materials containing crystalline $BaTiO_3$ should be possible by controlled crystallization of the respective glasses. Furthermore, it was envisaged to gather information on the structure and on the structural evolution in the case of the obtained multicomponent glasses in the system $Na_2O/BaO/TiO_2/B_2O_3/SiO_2/Al_2O_3$ where the concentrations of Na_2O and Al_2O_3 are varied. For this purpose, the method of Fourier-Transformed Infrared spectroscopy is used. The thermophysical characteristics of the obtained glasses, i.e., glass transition temperature, T_g, and crystallization peak maximum temperature, T_c, are determined by differential scanning calorimetry, DSC. Furthermore, the mechanical characteristics of the prepared materials are determined by using the method of depth-sensing indentation. Finally, the dependence between the determined structural peculiarities, thermal and mechanical properties is traced as a function of the changing sodium and aluminum oxide concentrations.

EXPERIMENTAL

Material

Reagent grade raw materials: Na_2CO_3, SiO_2, $BaCO_3$, $B(OH)_3$, $Al(OH)_3$ and TiO_2 were used for the synthesis of the glasses. The batches (60 g) were homogenized and melted in Pt-crucibles using a $MoSi_2$ furnace and a melting temperature of 1400°C for 1 h in air. Some of the melts were quenched on a Cu-block and, after quenching, transferred into a pre-heated graphite mould. The glasses cast into the graphite mould were transferred to a muffle furnace and kept at 450°C for 10 min. Then, the furnace was switched off and the samples were allowed to cool to room temperature with a rate of approximately 2 K min^{-1}.

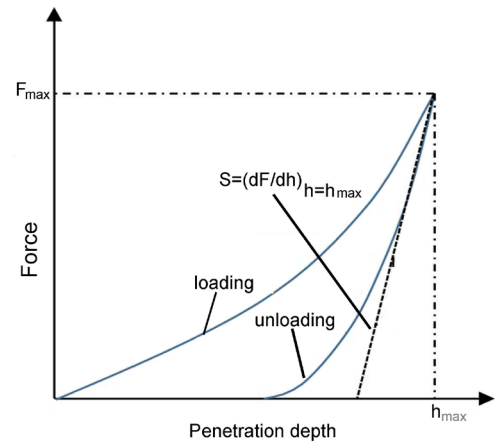

Fig. 1. Schematic representation of the indentation curve.

Characterization Methods

Determination of the thermophysical (DSC) and structural (IR-spectroscopy) characteristics of the glasses

The characteristic temperatures of the glasses, i.e., glass transition, T_g, and crystallization peak maximum, T_c, temperatures are obtained by utilizing DSC on powdered samples, powder fraction ≤ 350 μm. The powder is heated in an alumina crucible using a heating rate of 10 K/min and Al_2O_3 as reference. The thermal analyses are performed on a Linseis DSC PT-1600, LINSEIS Messgeräte GmbH, Germany.

The Infrared spectroscopy (IR) is carried out using an FTIR spectrophotometer VARIAN 600 on powdered samples pressed in KBr in the wavenumber range 400 cm^{-1} - 4000 cm^{-1}. The absorbance is recorded as function of the wavenumber at room temperature with an accuracy of ± 1 nm.

Depth-sensing indentation (DSI) for determination of the mechanical properties of the glasses

DSI is applied to study the obtained glasses [15, 16]. This method of controlled indentation is also known as instrumented indentation testing [17, 18]. For this type of analysis, the indentation tester measures the penetration depth, *h*, of the indenter tip as a function of the applied load, F, at a given constant loading speed. The result of the measurement is an indentation (F-h) curve, which gives the applied load versus the depth of penetration. A typical F-h curve is depicted schematically in Fig. 1. It consists of three parts: i) a loading part at load increase until reaching maximum load F_{max}; ii) an optional part of load holding when the load F_{max} is applied for a certain time which in the current study is chosen to be equal to 0, i.e., no holding was applied; iii) an unloading part at load decrease.

The obtained indentation curve enables the determination of various micro-mechanical characteristics. The first one is the universal hardness, HMV, calculated as $HMV = aF_{max}/h^2_{max}$, where h_{max} is the maximum depth obtained from the indentation curve, *a* is a constant depending on the indenter shape. For the measurement we used a Vickers pyramid with a = 3.8584. The HMV reveals how the material responds to plastic, elastic and viscoelastic deformation during the test, i.e., it characterises the total load-bearing capacity [18, 19]. The next parameter is the indentation hardness, H_{it}, determined according the Oliver-Pharr model as $H_{it} = F_{max}/(24.5h_c^2)$, where h_c is the depth of contact of the indenter with the test piece [20]. The indentation hardness is a measure for the resistance to permanent deformation. The depth h_c is found from $h_c = h_{max} - \varepsilon F_{max}/S$, where ε is a constant depending on indenter geometry. For Vickers pyramid ε=0.75. The parameter *S* is the stiffness, measured as a slope $S=dF/dh$ from the unloading part of the indentation curve at the maximum penetration depth. The unloading part of the dependence load-depth allows for determination of the indentation elastic modulus, E_{it} by using the relation $1/E_r - (1-\nu_s^2)/E_{it} + (1-\nu_i^2)/E_i$, where E_{it} is the experimental converted elastic modulus based on indentation contact, ν_s is the

Poisson ratio of the specimen, whereas E_i and v_i are the Young's modulus and Poisson's ratio for the indenter, respectively [21]. Elastic part of the indentation work, which is an indicator of the elasticity of the sample, is determined from $\eta_{it} = W_{el}/(W_{el} + W_{pl})$, where W_{el} and W_{pl} are the works for the elastic and plastic deformation during the indentation, respectively. The works are determined as the areas under loading and unloading parts of the indentation curve using $W=\int Fdh$.

The loading/unloading experiment was performed using a maximum force of 200 mN and a constant loading speed of 7.0067 mN s^{-1}. The load increasing was applied until the preset maximum force F_{max} = 200 mN was reached. No holding was applied for all specimens. Dynamic ultra-microhardness tester DUH-211S equipped with Vickers type indenter was used for recording of indentation curves. A set of micromechanical parameters was determined from the recorded indentation curves. For each sample 10 - 15 measurements were performed, and an average value for these parameters was calculated. All measurements were performed at room temperature, i.e., at about 22°C.

RESULTS AND DISCUSSION

The application of the traditional melt-quenching technique to the melts with the batch compositions **(**23.1-x)Na_2O/23.1BaO/23TiO_2/9.8B_2O_3/21SiO_2/xAl_2O_3 with x = 3 (Al 3), 7 (Al 7), 11 (Al 11) and 15 (Al 15) mol% resulted in the preparation of transparent glasses with only slight surface crystallization for the glass with x = 3 mol %. The color of the glasses varied from white-yellowish (3 mol % Al_2O_3) to light yellowish-pink (7 and 11 mol % Al_2O_3) turning up to light yellow for 15 mol % Al_2O_3.

In order to characterize the structure, thermal and mechanical properties of the glasses and to trace the influence of the changing ratio [Na_2O]/[Al_2O_3], DSC, IR and DSI studies are further performed.

DSC Measurements

The T_g and T_c values for the four glasses are obtained while heating up the powdered samples with a rate of 10 K min^{-1}. The T_g and T_c values determined from the thermograms are plotted as function of the alumina concentration in Fig. 2. It could be seen that the increasing Al_2O_3 concentration leads to an increase

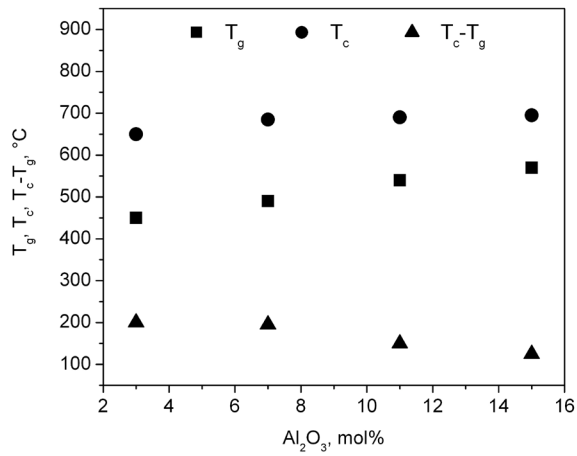

Fig. 2. Dependencies of T_g, T_c and T_c-T_g on the Al_2O_3 concentration.

of both the T_g and T_c values from 450°C to 570°C and from 660°C to 695°C, respectively. Such a tendency is expected in case of increasing concentrations of alumina in a sodium-borosilicate glass with high Na_2O concentration because the addition of Al_2O_3 will initially lead to stabilization of the glass network due to tetrahedral coordination of the Al^{3+} ions with oxygen ions, i.e., the formation of AlO_4^- structural units [1, 22 - 25]. After some threshold concentration is reached, the transition from the per-alkali to the per-aluminous range of concentrations occurs, the Al^{3+} ions will tend to form octahedra with the O^{2-} ions and thus, lead to a depolymerization of the glass network [23 - 25]. In the present study, as seen in Fig. 2, the transition to the per-aluminous range of concentrations is most probably not reached for the investigated alumina concentrations. Furthermore, the difference T_c-T_g, which is often suggested as a measure for the tendency of a melt to solidify as a glass, is also shown in Fig. 2. As seen in Fig. 2, the effect of the alumina concentration on T_c-T_g is just the opposite as that on T_g and T_c - the largest difference is obtained for the glass with the lowest Al_2O_3 concentration, i.e., Al 3 and the next composition with 7 mol % Al_2O_3 has basically the same T_c-T_g value, while it is smallest for the glass Al 15. This phenomenon can be explained with the extremely low concentration of the glass-forming oxides in the developed series of compositions, here boron oxide and silica - in total 30.8 mol %. The latter results in the preparation of the so-called invert glass as described by Stevels and Trap

in [26]. Invert glasses solidify as amorphous solids not because of the presence of a continuous glass network with high network connectivity. By contrast, they possess many NBOs due to the large concentration of network-modifiers such as Na_2O and BaO. If now, starting from the sample with 3 mol % Al_2O_3, the concentration of alumina is increased at the expense of the Na_2O concentration, aluminum is incorporated as AlO_4^- tetrahedra which negative charge is compensated by the network modifier cations. That means, the number of networks forming compounds increases (aluminum in tetrahedral coordination), while that of the NBOs decreases, because Na^+ is increasingly incorporated to compensate the charge of the AlO_4^- tetrahedra.

Infrared (IR) spectroscopy measurements

Fig. 3 shows infrared spectra recorded from powdered glasses using the KBr technique. The survey of the IR-spectra in the wavenumber range 400 cm^{-1} - 4000 cm^{-1} is given in Fig. 3(a) while in Fig. 3(b) only the wavenumber range 400 cm^{-1} - 2000 cm^{-1} concerning the structure of the studied samples is shown.

The IR-spectra of the glasses could be discussed by dividing them into 2 regions - from 400 cm^{-1} to 700 cm^{-1} and from 700 cm^{-1} to 1500 cm^{-1} which are important for the characterization of the structure and its changes with the Na_2O/Al_2O_3 ratio. The data from Fig. 3 is summarized in Table 1. The attribution of the wavenumbers in Table 1 was done according to [27 - 33]. The range from 1500 cm^{-1} to 4000 cm^{-1} contains the features typical for the IR-spectra of most sodium aluminoborosilicate glasses. The broad absorption band between 3400 cm^{-1} and 3500 cm^{-1} is due to absorbed water, an absorption band at approximately 2320 cm^{-1} to 2380 cm^{-1} is attributed to CO_2 in the gas atmosphere and sharp absorptions bands at 2800 cm^{-1} to 2900 cm^{-1} caused by C-H valence vibrations of trace quantities of organics present in the measuring camera atmosphere of the spectrometer.

According to Fig. 3, in the first region, 400 cm^{-1} - 700 cm^{-1}, a well resolved small absorption peak at 418 cm^{-1} is observed for the glasses Al 7 to Al 15, while for the glass Al 3 it is missing. This peak is attributable to bending vibrations of the O-Si-O bonds. Vice versa, for the Al 3 sample, a hump between 540 cm^{-1} and 610 cm^{-1} is observed which might be associated with the presence of some pre-nucleation clusters. Possibly, $BaTiO_3$ will precipitate from these clusters. This hump is slightly expressed and almost invisible for the other three glasses which could serve as evidence for the phase separation of the Al 3 glass which, however, is not present in the rest of the glasses from the compositional series studied [27 - 29]. Furthermore, a small intensity but also well-visible peak is resolved at 616 cm^{-1} - 617 cm^{-1} for the glasses Al 7 - Al 15 and again missing for the Al 3 glass. This peak is attributed to deformation vibrations of the SiO_4 units typical for the absorption spectra of orthosilicates [30, 31]. For all four alumina concentrations, a group of three peaks is detected at 650 cm^{-1}, 670 cm^{-1} and 682 cm^{-1} - the peak at 682 cm^{-1} again being very weak and not well-resolved for the Al 3 glass. This group of peaks is suggested to correspond

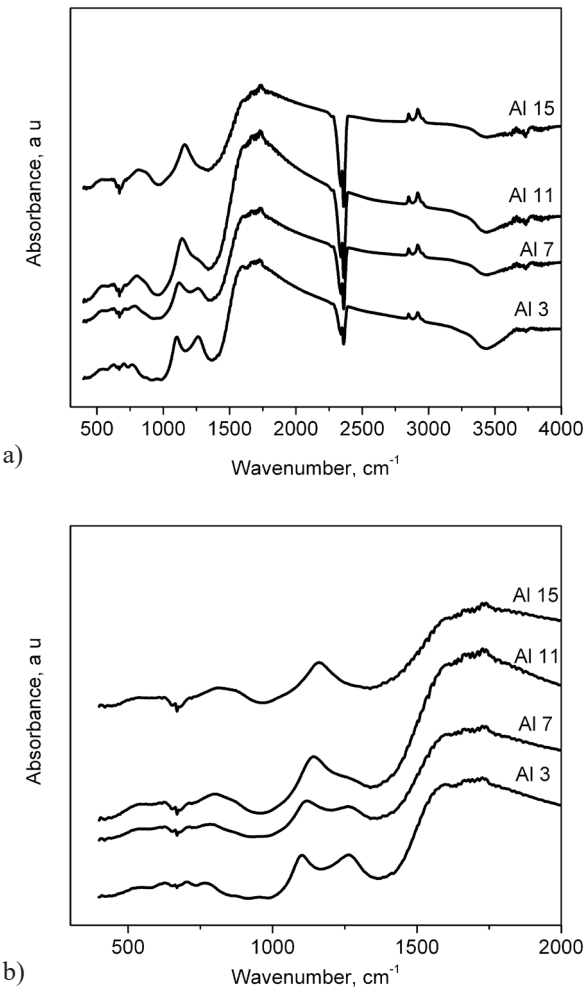

Fig. 3. IR-spectra of the glasses from the series $(23.1\text{-}x)Na_2O/23.1BaO/23TiO_2/9.8B_2O_3/21SiO_2/xAl_2O_3$, x = 3 (Al 3), 7 (Al 7), 11 (Al 11) and 15 mol%(Al 15)- a) spectral range 400-4000 cm^{-1} and b) spectral range 400 cm^{-1} - 2000 cm^{-1}.

Table 1. IR-bands assignment for the glasses Al 3, Al 7, Al 11 and Al 15.

Type of band	**Type of vibration**	**IR peak in cm^{-1}**			
		Al 3	**Al 7**	**Al 11**	**Al 15**
O-Si-O O-B-O Si-O-Si	bending bending rocking	442, 473	439, 470	457	456
Si-O-Si $BaTiO_3$	rocking	564	566	524	562
O-Si-O/B-O-B bending	BO_3^- bending	672	677	669	669
B-O-B bending	B-O-B, B-O-Si stretching	732	735	700	717
Si-O-Si, symmetric BO_4		856	792, 844		848
Si-O BO_4,	Si-O stretching Si-O-Si, BO_4^- stretching	919	918	960	988
Si-O	Si-O stretching	1016	1009	1073	1090
BO_4 diborate	B-O BO_4^-stretching	1062	1059		
Si-O-Si stretching	interconnected SiO_4, BO_3 units with NBOs	1136	1151	1127	
B-O asymm orthoborate	B-O stretching BO_3	1205	1217	1203	1225
BO_3 asymm stretching	isolated and interconnected SiO_4, BO_3 units with NBOs	1319	1367	1297	1340
B-O asymm stretching	BO_3	1419	1445	1421	-
O=C=O	pollution	2320-2380	2320-2380	2320-2380	2320-2380
C-H	stretching	2800-2900	2800-2900	2800-2900	2800-2900
O-H	stretching	3200-3500	3200-3500	3200-3500	3200-3500

again to bending vibrations of the O-Si-O groups but could also be due to the presence of boron oxide in the glass compositions and thus, the occurrence of B-O vibrations in BO_3 or BO_4^- structural units [30]. In the second wavenumber sub-range of interest - 700 cm^{-1} - 1500 cm^{-1}, samples Al 3 and Al 7 show a peak of small intensity at 735 cm^{-1} which could correspond to the B-O vibration in the BO_4 polyhedron and is missing in the absorption spectra of the glasses Al 11 and Al 15. In the range 780 cm^{-1} - 1160 cm^{-1}, a group of three overlapping peaks for the glasses Al 3 and Al 7 is observed while in the same region, only two peaks could be resolved for the glasses Al 11 and Al 15. The wavenumber range 760 cm^{-1} - 850 cm^{-1} is characteristic for the occurrence of the stretching vibrations of isolated SiO_4 groups. In the range 840 cm^{-1} - 1200 cm^{-1}, vibrations of both isolated and interconnected SiO_4 or AlO_4^- groups are observed. The three peaks for the glass Al 3 are centered at approximately 845 cm^{-1}, 907 cm^{-1} and 992 cm^{-1} while for the Al 7 sample their peaks are situated at approximately 845 cm^{-1}, 915 cm^{-1} and 987 cm^{-1} and a fourth peak with lower intensity at approximately 1045 cm^{-1} starts to emerge. The three peaks in the range from 840 cm^{-1} to 995 cm^{-1} could be attributed to the occurrence of both isolated and interconnected SiO_4 tetrahedra. But also, the attribution of these absorption peaks to Al-O and B-O stretching vibrations of isolated AlO_4^- and BO_4^- groups, which are charge-compensated by Na^+ ions, should be considered [27]. However, as reported in former studies [27], in the IR-spectra of the studied samples, a large number of BO_3 triangles are present in the wavenumber range 1200 cm^{-1} - 1600 cm^{-1}, which correspond to B-O stretching vibrations [34, 35]. The fourth peak at 1045 cm^{-1} is resolved close to the group of two peaks - at 1052 cm^{-1} (Al 11) and 1072 cm^{-1} (Al 15), which should belong to SiO_4 tetrahedra in an amorphous network. The two very intense absorption peaks at 957 cm^{-1} (Al 11) and 967 cm^{-1} (Al 15) could be attributed either to the existence

of interconnected SiO_4 tetrahedra or could be explained with the presence of Al-O and B-O stretching vibrations of isolated AlO_4 and BO_4 groups, which are charge-compensated by Na^+ ions. The presence of these peaks in these two glasses correlates with the results reported above where increasing alumina concentrations lead to higher glass-transition and crystallization temperatures. Furthermore, in the Al 3 glass, relatively intense and very well resolved absorption double peaks centered at 1169 and 1206 cm^{-1} and a second also intense and very broad peak at 1370 cm^{-1} are observed. These peaks are attributable to isolated, interconnected SiO_4 tetrahedra and BO_3 triangles containing non-bridging oxygens, respectively [30, 31]. By analogy, in the IR-spectrum of the Al 7 glass, a similar group of three peaks is observed which, however, possess much lower intensities. The first is a single and very broad peak at 1191 cm-1, due to its relatively low intensity, it is difficult to speculate whether it is a superposition of two or three peaks. At approximately 1342 cm^{-1}, a broad and intense peak occurs, which is assigned to interconnected SiO_4 groups and BO_3 triangles. The next peak at 1342 cm^{-1} overlaps with the second peak at 1426 cm^{-1} and can again be associated to the occurrence of BO_3 triangles containing non-bridging oxygen ions. For the glasses Al 11 and Al 15, the peak at 1169 - 1191 cm^{-1} observed for the Al 3 and Al 7 glasses is missing but a new combination of overlapping peaks centered at 1127 cm^{-1} and 1342 cm^{-1} (Al 11) and 1259 cm^{-1} and 1344 cm^{-1} (Al 15) appears which is again attributed to interconnected SiO_4 groups and BO_3 triangles, respectively. It is worth to note here that for the Al 11 and especially, Al 15 sample the peaks at 1150 cm^{-1} - 1450 cm^{-1} become very wide and their maxima are slightly shifted to smaller wavenumbers which could probably be explained by the occurrence of SiO_4 but also by the presence of AlO_4 interconnected groups which correlates well with the higher alumina concentration for these glasses.

The former investigations on the microstructure of glass-ceramics obtained from the same glasses shows that Al 3 is most probably phase-separated while the other 3 glasses, Al 7 - Al 15 are not [36]. Then, in the Al 3 glass, two phases are present - one enriched in Ba and Ti and a second one where the other glass components are enriched. This idea of occurrence of phase separation is in good agreement with the data for oxide glasses with a smaller number of components [1]. It should be noted that in the glasses, a high concentration of clusters with a structure and chemical composition similar to $BaTiO_3$ are supposed to exist [27 - 29]. It is further suggested that these clusters serve as pre-nucleation complexes from which after applying an appropriate thermal treatment, the barium titanate nuclei will be formed. Thus, volume crystallization of the $BaTiO_3$ phase with a high density and relatively uniform distribution of the precipitated crystals is achieved. This high nucleation rate will result in nano-sized mono-dispersed crystals which is due to the almost immediate and simultaneous crystal growth in the glass matrix as long as Ostwald ripening is negligible. The charge compensation is predominantly carried out by the Na^+ ions, but also by Al^{3+} ions. The chemical composition of the residual glass changes during the course of the crystallization process and concentration gradients from the type „core-shell" will be formed around the growing crystals. For some of the glasses and under certain conditions, these shell regions will lead to the preservation and even slight increase of the number of the BO_3 triangles while the number of BO_4 tetrahedra will decrease. After the crystallization process is completed, the concentration gradient regions around the growing crystals will disappear as a result of the occurring diffusion-controlled processes and the number of the BO_3 triangles will slightly decrease.

Although the nominal glass composition is consisting of 7 components, actually, in the real composition there are even more components due to the adsorbed water as evidenced from the absorption band in the range 3400 cm^{-1} - 3500 cm^{-1} in Fig. 3. It is also possible that at the surface some amount of $BaCO_3$ is formed due to chemisorption of CO_2 from the environment and the high BaO concentration in the glasses.

Micromechanical properties

The mechanical properties of amorphous and crystalline materials are related to their thermophysical and electrical properties, and thus, determine their potential application. For this reason, the micromechanical properties of the four synthesized glasses are studied and the obtained indentation curves are shown in Fig. 4. The indentation curves from Fig. 4 reveal that the sample Al 3 is characterized by the highest penetration depth for equal test parameters during the loading/unloading experiment and as a result exhibits the least resistance towards the indenter penetration, With the increasing

alumina concentration, i.e., for the samples Al 7-Al 15, the resistance towards the penetration of the indenter increases and thus, these samples seem to be harder. The results shown in Fig. 4 could be explained having in mind the data from the DSC and the IR-spectroscopy analyses. The samples Al 3 have lowest alumina concentration and are phase separated and thus the Al^{3+} ions tend to act as network modifiers which loosens the glass network and makes the indenter penetration easier [27, 36]. Increasing alumina concentration results in strengthening of the glass network due to the occurrence of AlO_4^- structural units as witnessed from increasing T_g values. The data from Fig. 4 allows to suggest that most probably, the largest number of tetrahedrally coordinated Al^{3+} ions correspond to the glass Al 11 while the further increase of the alumina concentration will lead to the occurrence of Al^{3+} which are octahedrally coordinated and will again lead to weakening of the glass network.

Information about the universal hardness (HMV), indentation hardness (H_{it}) and the elastic indentation moduli, E_{it} for the tested samples was extracted from the indentation curves and is compared for the different samples in Figs. 5(a) and 5(b). As seen in Fig. 5(a), both the universal (*HMV*) and indentation (H_{it}) hardness of the glasses increase for alumina concentrations up to 11 mol %, while for 15 mol % Al_2O_3, both moduli decrease again. This behavior is attributable to the observation that in oxide glasses with varying $[Na_2O]/[Al_2O_3]$ concentrations, the network connectivity and the viscosity is highest for ratios close to 1, while for values of the ratio lower or larger than unity, the network connectivity and viscosity decreases [23 - 25]. The samples Al 15 show the smallest elastic resistance against the penetrating pyramid, i.e. it is the most plastic from all tested glasses. Nevertheless, the data in Fig. 5(a) witnesses that the hardness of the samples Al 11 and Al 15 is higher than that of the glasses Al 3 and Al 7 which correlates with the observations from the IR spectra that the higher alumina concentration will lead to a larger number of TO_4 building interconnected units, where T = Al^{3+}, Si^{4+}. In Fig. 5(b), the elastic moduli of the four tested glasses are presented. They were obtained as tangents to the initial part of the unloading section of the indentation curves. The moduli of the glasses Al 3 to Al 15 follow the same trend within the margins of error as the hardness which can again be explained by the structure and the resulting viscosity. Namely, the

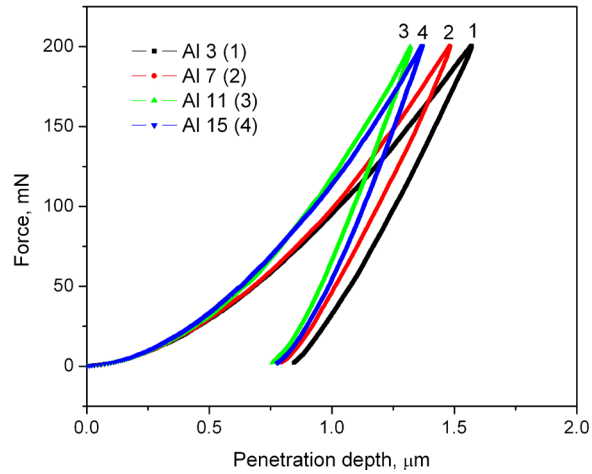

Fig. 4. Indentation curves for the four tested glasses: Al 3 (1), Al 7 (2), Al 11 (3) and Al 15 (4).

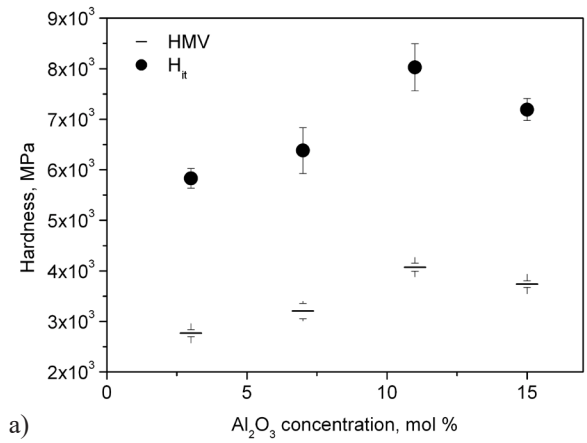

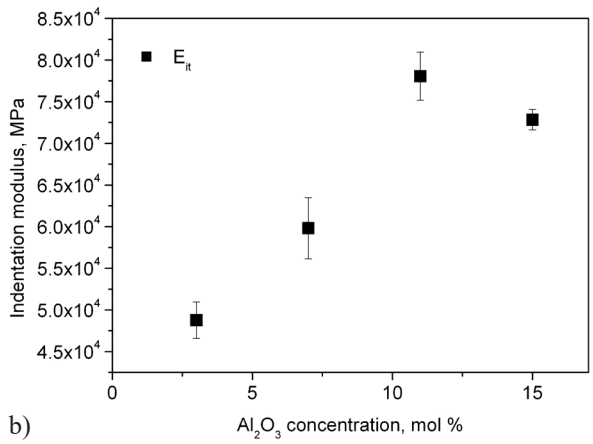

Fig. 5. a) Universal hardness (HMV), indentation hardness (H_{it}); b) elastic indentation moduli, E_{it}, for the tested samples.

glasses Al 3 and Al 7 have smaller number of BO_4 and most probably, larger number of BO_3 triangles in their structure compared to the samples Al 11 and Al 15 and thus, their hardness is smaller. In the samples with higher alumina concentration - Al 11 and Al 15 - all Si^{4+} and most probably some of the Al^{3+} ions occupy T_d positions. The respective tetrahedra are part of the amorphous network which is supported by the IR spectra analysis as shown in Fig. 3. Furthermore, for Al 3 and Al 7, a peak of small intensity at 735 cm^{-1} (Fig. 3(b)) which could correspond to the B-O vibration in the BO_4 tetrahedron is present, while it is missing in the absorption spectra of the glasses Al 11 and Al 15. Nevertheless, all the glasses are characterized by a relatively large number of BO_3 units corresponding to NBOs which again corresponds to the above observations in case of the increasing alumina concentration. Furthermore, in the range 780 cm^{-1} - 1160 cm^{-1}, peaks corresponding to the stretching vibrations of isolated and interconnected SiO_4 and possibly, AlO_4 groups for the glasses Al 3 and Al 7 are observed, while in the same region only two peaks shifted to higher wavenumbers could be resolved for the glasses Al 11 and Al 15. So, it may be suggested that the observed micromechanical properties of the studied glasses Al 3 - Al 15 are the result of a very complicated and evolving structure in which the presence of SiO_4 and BO_4 units as part of the amorphous network competes with the emerging AlO_4 tetrahedra which are also most probably part of the glass network with the increasing alumina concentrations.

The graph in Fig. 6 compares the elasticity of the four tested glasses. Elastic part of indentation work, η_{it} differs from the tendency in the hardness estimation - the samples Al 3 and Al 7 possess slightly higher elastic components while the Al 15 sample is characterized by the smallest elasticity. The above statements are supported by the information shown in Figs. 7(a) and 7(b) where the dependencies of the HMV, and H_{it} are shown as function of the T_g and T_c-T_g values for the four glasses. As seen from Fig. 7(a), both HMV and H_{it} increase with the increasing T_g which corresponds also to the increasing alumina concentration and probably, total number of BOs. Besides, the estimated values of the indentation moduli are highest for the sample Al 11 and then slightly decrease for Al 15 glass, cf. Fig. 5(b). This observation is consistent with the idea reported in [23 - 25] that the viscosity of an oxide glass is highest for

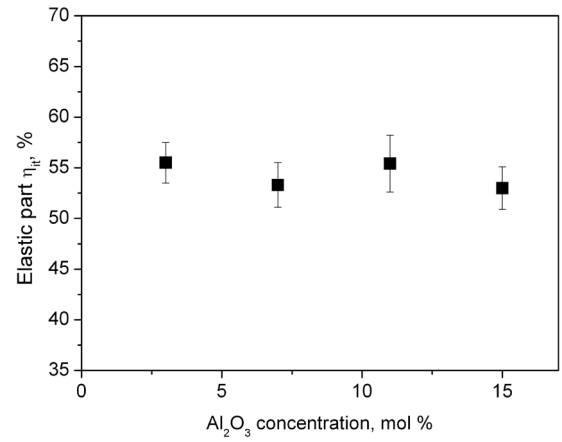

Fig. 6. Graphical dependence of elastic part of the indentation work on the alumina concentration.

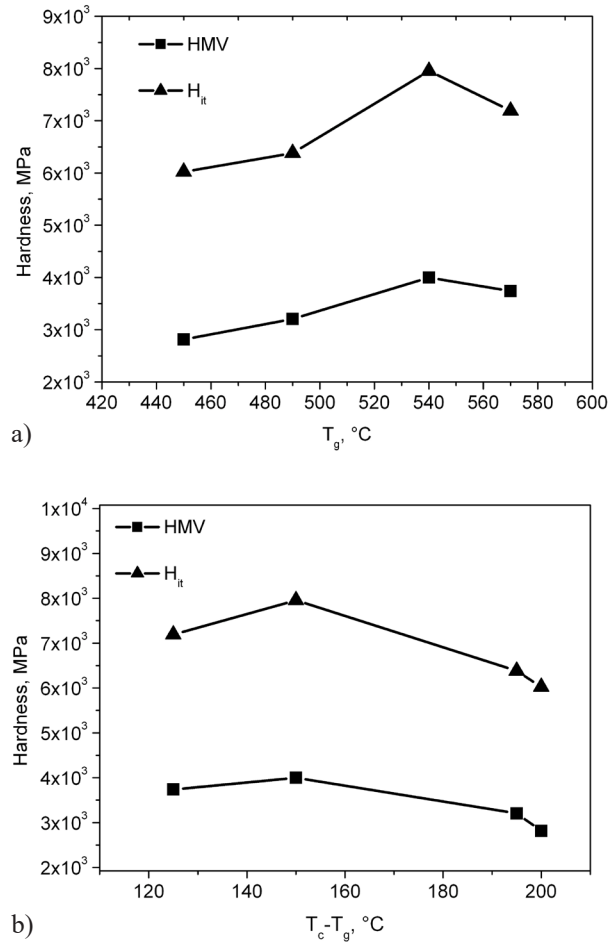

Fig. 7. a) HMV and H_{it} dependence on T_g without applied holding under load; b) HMV and H_{it} dependence on T_c-T_g without applied hold under load.

almost equal alumina and sodium oxide concentrations. The slight decrease of the indentation moduli could be also due to the slight increase of the number of NBOs in the Al 15 glass compared to the Al 11 sample. Similar is the tendency in the dependencies microhardness vs. the difference T_c-T_g. Here again the highest moduli are characteristic for the glass Al 11 and then for the sample Al 15. The respective values of HMV and H_{it} are much lower in case of the glasses Al 3 and Al 7.

CONCLUSIONS

In the present work, the mechanical and thermo-physical properties, as well as the structure of the glasses prepared in the system (23.1-x)Na_2O/xAl_2O_3/ 23.1BaO/23TiO_2/9.8B_2O_3/21SiO_2 for x = 3, 7, 11 and 15 mol % as a dependence on the varying ratio between the alumina and sodium oxide concentrations are studied. The increasing alumina concentration results in improved glass formation, i.e., increasing glass transition temperature and occurrence of AlO_4 structural units in the glass network as confirmed by the IR spectra. Furthermore, the comparison of the determined mechanical characteristics of the studied glasses reveals that again the increasing alumina concentration leads to higher hardness.

Acknowledgements

This work is financially supported by contract KP06-06-N28/1 with the Bulgarian National Science Fund.

REFERENCES

1. W. Vogel, Glasschemistry, Springer-Verlag, Heidelberg, New York, 2nd edition, 1985.
2. R. Harizanova, I. Avramova, Z. Cherkezova-Zheleva, D. Paneva, R. Kukeva, R. Stoyanova, I. Gugov, I. Mihailova, D. Tzankov, M. Georgieva, G. Avdeev, C. Bocker, C. Rüssel, J. Non-Cryst. Solids, 546, 2020, 120273, DOI: 10.1016/j.jnoncrysol.2020.120273.
3. R. Harizanova, S. Slavov, L. Vladislavova, L. C. Costa, G. Avdeev, C. Bocker, C. Rüssel, Barium titanate containing glass-ceramics – The effect of phase composition and microstructure on dielectric properties, Ceramics International, 46, 2020, 24585-24591, doi.org/10.1016/j.ceramint.2020.06.247
4. A. Bhargava, R.L. Snyder, R.A. Condrate, Preparation of $BaTiO_3$ glass-ceramic in the system Ba-Ti-B-OII, Mater. Lett., 7, 1988, 190-196.
5. Z. Libor, S. A. Wilson, Q. Zhang, Rheological properties of magnetic and electro-active nano-particles in non-polar liquids, J. Mater. Sci., 46, 2011, 5385-5393.
6. J.F. Capsal, E. Dantras, L. Laffont, J. Dandurand, C. Lacabanne, Nanotexture influence of BaTiO3 particles on piezoelectric behaviour of PA 11/BaTiO3 nanocomposites, J. Non-Cryst. Solids, 356, 2010, 629-634.
7. H.T. Langhammer, T. Müller, T. Walther, R. Böttcher, D. Hesse, E. Pippel, S.G. Ebbinghaus, Ferromagnetic properties of barium titanate ceramics doped with cobalt, iron, and nickel, J. Mater. Sci., 51, 2016, 10429-10441.
8. G.P. Du, Z.J. Hu, Q.F. Han, X.M. Qin, W.J. Shi, Effects of niobium donor doping on the phase structures and magnetic properties of Fe doped BaTiO3 ceramics, J. Alloys&Compounds, 492, 2010, L79-L81.
9. R.P. Maiti, S. Basu, S. Bhattacharya, D. Chakravorty, Multiferroic behavior in silicate glass nano composite having a core-shell microstructure, J. Non-Cryst. Solids, 355, 2009, 2254-2259.
10. M.M. Gomaa, H.A. Abo-Mosallam, H. Darwish, Electrical and mechanical properties of alkali barium titanium aluminoborosilicate glass-ceramics containing strontium or magnesium, J. Mater. Sci: Mater. Electron., 20, 2009, 507-516, DOI 10.1007/s10854-008-9758-2.
11. S.S. Ryu, H.T. Kim, H.J. Kim, S. Kim, Characterization of mechanical properties of $BaTiO_3$ ceramic with different types of sintering aid by nanoindentation, J. Ceram. Soc. Japan, 117, 2009, 811-814.
12. A.K. Himanshu, S.K. Bandyopadhyay, P. Sen, D.C. Gupta, R. Chakraborty, A.K. Mukhopadhyay, B.K. Choudary, T.P. Sinha, Dielectric and micromechanical studies of barium titanate substituted (1-y)Pb($Zn_{1/3}Nb_{2/3}$) O_{3-y} PT ferroelectric ceramics, Indian Journal of Pure and Applied Physics, 48, 2010, 349-356.
13. S. Suresh, A.E. Giannakopoulos, S. Sridhar, U. Ramnamurty, Indentation of piezoelectric ceramics: Theory, experiment and applications, Mat. Res. Soc. Symp. Proc., v. 604, Warrendale, Pennsylvanya,Materials Research Society, 2000.

14. P. Vinothkumar, M. Dhavamurthy, M. Mohapatra, P. Murugasen, The effects of Ba^{2+} addition in the $LiCO_3$–Mn_2O_3–B_2O_3 glass structure on electrochemical and physical characterizations, J Mater Sci: Mater Electron, 32, 2021, 22548-22560.
15. G.M. Pharr, Measurement of mechanical properties by ultra-low load indentation, Mater. Sci. Eng. A253, 1998, 151-159.
16. A.C. Fischer-Cripps, Introduction to contact mechanics, 2nd ed. New York: Springer, 2007.
17. J. Hay, Introduction to instrumented indentation testing, Exp. Techniques, 33, 2009, 66-72.
18. G. Zamfirova, Indentation Methods for the Characterization of Carbon-Based Polymer Nanocomposites in: Carbon-Based Polymer Nanocomposites for Environmental and Energy Applications, Ed. A. F. Ismail and P. S. Goh, Elsevier, pp 79-111, 2018.
19. R.V. Tatiraju, C. S. Han, S. Nikolov, Size dependent hardness of polyamide/imide, The Open Mechanics Journal, 2, 2008, 89-92.
20. W.C. Oliver, G.M. Pharr, An improved technique for determining hardness and elastic modulus using load and displacement sensing indentation experiments, J. Mater. Res., 7, 1992, 1564-1583.
21. W.C. Oliver, G.M. Pharr, Measurement of hardness and elastic modulus by instrumented indentation: Advances in understanding and refinements to methodology, J. Mater. Res., 19, 2004, 3-20.
22. K. El-Egili, Infrared studies of Na_2O–B_2O_3–SiO_2 and Al_2O_3–Na_2O–B_2O_3–SiO_2 glasses, Phys. B, 325, 2003, 340-348.
23. S. Hornschuh, B. Messerschmidt, T. Possner, U. Possner, C. Rüssel, Silver ion exchange in glass of the system Na_2O-Al_2O_3-B_2O_3-SiO_2, J. Non-Cryst. Solids, 347, 2004, 121-127.
24. L. Hong, P. Hrma, J. D. Vienna, M. Qian, Y. Su, D.E. Smith, Effects of Al_2O_3, B_2O_3, Na_2O and SiO_2 on nepheline formation in borosilicate glasses: chemical and physical correlations, J. Non-Cryst. Solids, 331, 2014, 202-216.
25. D. Benne, C. Rüssel, M. Menzel, K. Becker, The effect of alumina on the Sn^{2+}/Sn^{4+} redox equilibrium and the incorporation of tin in $Na_2O/Al_2O_3/SiO_2$ melts, J. Non-Cryst Solids, 337, 2014, 232- 240.
26. H.J.L. Trap, J.M. Stevels, Physical properties of invert glasses, Glastech. Ber. 32K, 1959, 31-56.
27. R. Harizanova, I. Gugov, I. Avramova, I. Mihailova, G. Avdeev, C. Rüssel, Chapter 26: Phase composition and spectroscopic characterization of barium titanate containing glass ceramics, Booktitle: Nanoscience and Nanotechnology in Security and Protection against CBRN Threats, Series title: NATO Science Peace Security Ser. B, ISBN:978-94-024-2017-3.
28. S. Wada, T. Suzuki, T. Noma, Role of lattice defects in the size effect of barium titanate fine particles, J. Ceram. Soc. Japan, 104, 1996, 383-392.
29. S. Wada, H. Chikamori, T. Noma, T. Suzuki, T. Tsurimi, Synthesis of nanometer-sized barium titanate crystals using a modified low temperature direct synthesis method and their characterization, J. Ceram. Soc. Japan, 108, 2000, 728-735.
30. V. Dimitrov, Y. Dimitriev, Structural analysis (Spectral Methods), UCTM Publishing house, Sofia, 2009, in Bulgarian.
31. I.I. Plusnina, Infrared spectra of minerals, MGU, Moscow, 1977.
32. Y. Lai, Y. Zeng, X. Tang, H. Zhang, J. Han, H. Su, Structural investigation of calcium borosilicate glasses with varying Si/Ca ratios by infrared and Raman spectroscopy, RSC Adv., 6, 2016, 93722.
33. R. Ciceo Lucacel, T. Radu, A.S. Tătar, I. Lupan, O. Ponta, V. Simon, The influence of local structure and surface morphology on the antibacterial activity of silver-containing calcium borosilicate glasses, J. Non-Cryst. Solids, 404, 2014, 98-103.
34. G. El-Damrawi, K. El-Egili, Characterization of novel CeO_2/B_2O_3 glasses, structure and properties, Physica B, 299, 2001, 180-186.
35. N.O. Dantas, W.E.F. Ayta, A.C.A. Silva, N.F. Cano, S.W. Silva, P.C. Moraisc, Effect of Fe_2O_3 concentration on the structure of the SiO_2–Na_2O–Al_2O_3–B_2O_3 glass system, Spectrochimica Acta Part A, 81, 2011, 140-143.
36. R. Harizanova, D. Tatchev, G. Avdeev, C. Bocker, D. Karashanova, I. Mihailova, I. Gugov, C. Rüssel, Investigation on the crystallization behaviour of sodium-alumino borosilicate glasses with high concentrations of Ba and Ti, Bulg. Chem. Comm., 49A, 2017, 119-125.